Experimental Investigation of Multielement Airfoil Ice Accretion and Resulting Performance Degradation

M. G. Potapczuk*
NASA Lewis Research Center, Cleveland, Ohio 44135
and
B. M. Berkowitz†
Sverdrup Technology, Inc., Brook Park, Ohio 44142

An investigation of the ice accretion patterns and performance characteristics of a multielement airfoil was undertaken in the NASA Lewis Icing Research Tunnel. Several configurations were examined to determine the pattern of ice accretion and to provide information for code validation purposes. The testing included glaze, rime, and mixed icing regimes. Tunnel cloud conditions were set to correspond to those typical of the operating environment for commercial transport aircraft. Measurements acquired included ice profile tracings and aerodynamic forces both during the accretion process and in a postaccretion evaluation over a range of angles of attack. Substantial ice accretions developed on the main wing, flaps, and slat surfaces. Force measurements indicate severe performance degradation, especially near $C_{L\max}$, for both light and heavy ice accretions. Frost was seen on the lower surface of the airfoil. The cruise wing configuration provided a test case for evaluation of ice accretion and performance analysis codes. The comparison of the calculations to the experiment was encouraging.

Introduction

SEVERAL studies of ice accretions and resulting performance losses for typical airfoil profiles have been completed.[1-6] Most studies to date, with the notable exception of Ingelman-Sundberg et al.,[7] have been for single-element airfoils such as the NACA0012 profile. The use of slats and flaps has the potential for development of significant ice accretions at many locations on an airfoil other than the leading edge. In an effort to document these accretions and their effects on airfoil performance, icing tests were performed on a multielement model representing a Boeing 737 wing section. This model, configured for four simulated flight conditions, was tested in the NASA Lewis Icing Research Tunnel (IRT) while mounted in a horizontal position between two splitter walls, as shown in Fig. 1. The configurations tested are shown in Figs. 2-11. The cruise configuration, the airfoil with slats and flaps fully retracted, is shown in Figs. 2-4. The airfoil geometries shown in Figs. 5-11 have varying slat and flap conditions and correspond to various high-lift configurations.

The conditions of the test were set to attempt reproduction of natural icing conditions for this airfoil during hold and approach situations, as specified in the Federal Aviation Regulations, Part 25 (FAR-25) specifications for commercial aircraft. This was not always possible given the restrictions imposed by the scale of the models and the capabilities of the IRT. In several cases, the spray durations were extended in order to accumulate ice of sufficient quantities to allow tracings to be feasible. Additionally, it was desired to obtain results for glaze, rime, and mixed conditions in order to develop an understanding of how these may impact the several configurations examined. Glaze ice accretions occur at warm temperatures and high cloud liquid water content whereas rime ice accretions occur at cold temperatures and low cloud liquid water content. Glaze ice accretions can produce large protuberances called horns at locations slightly downstream of the stagnation region. Mixed ice accretion has a glaze ice core at the stagnation region with surrounding layers of rime ice. Further explanation of these differences is found in Ref. 6.

A key objective of this test was to provide substantial experimental information for evaluation of ice accretion codes (e.g., LEWICE) and aerodynamic performance codes, especially for future versions of these codes that may be modified for multielement airfoils. In support of this objective, ice shape tracings were taken for each test run at several locations along the airfoil span. The spanwise variations in ice shape geometry indicate the basic uncertainty inherent in characterizing airfoil ice accretions. The variation of the force measurements due to the ice shape may also be used to evaluate the accuracy of the aerodynamic performance codes contemplated for use in predicting iced airfoil behavior. The changes in performance as a function of time can be used to study the dynamics of the ice accretion process. This cannot be done with ice tracing methods since stopping and restarting the spray cloud would result in an ice shape somewhat different than that produced by a continuous spray for the same time period.

Test Description

This test program was conducted in the NASA Lewis IRT. The IRT is a closed-loop, subsonic wind tunnel with a 0.82×2.74-m, solid-wall test section. The maximum test section velocity is 135 m/s with no blockage. The IRT airstream temperature is controlled by a 2100-ton Freon cooling system that allows the total temperature to range between 0 and $-35°C$. Atmospheric icing clouds are simulated in the tunnel by spraying water droplets into the cold airstream slight upstream of the contraction section. Calibrated clouds may be generated with liquid water contents ranging from 0.5 to over 2 gm/m^3 and with volume median droplet diameters ranging from 10 to 20μm.

The test article was a 0.18-scale model of a Boeing 737-200ADV wing wing section. The cruise configuration had a

Presented as Paper 89-0752 at the 27th Aerospace Sciences Meeting, Reno, NV, Jan. 9-12, 1989; received March 25, 1989; revision received Jan. 13, 1990.

*Aerospace Engineer. Member AIAA.
†Aircraft Icing Engineer, Lewis Research Center Group.

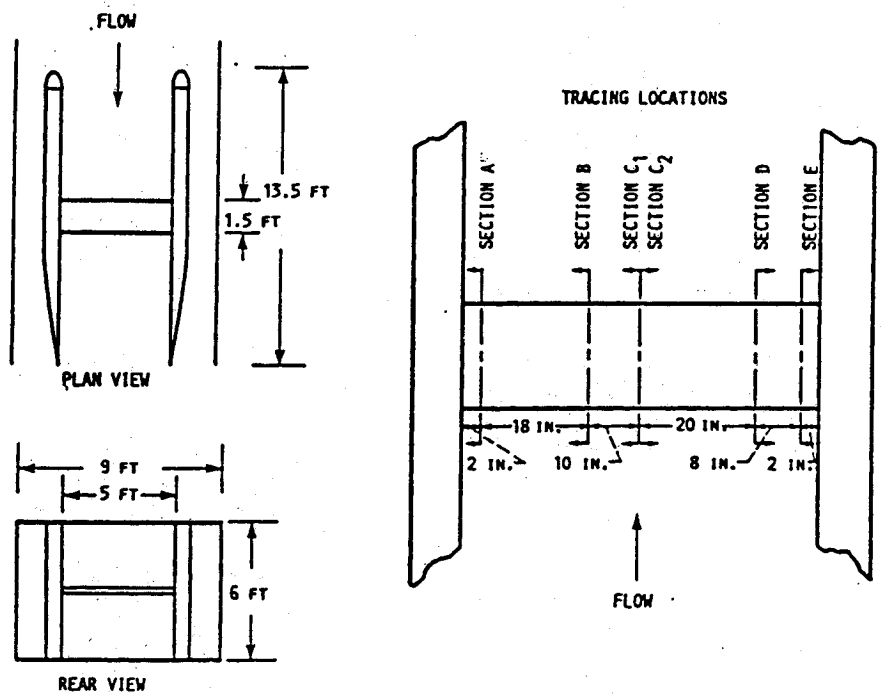

Fig. 1 Splitter wall configurations for two-dimensional wing model.

chord length of 45.72 cm and a span of 1.52 m. The model was mounted horizontally between two splitter walls that spanned the height of the tunnel test section. The model could be rotated about its spanwise axis using a turntable mounted in the splitter walls. This allowed variation of the angle of attack both during and after the duration of the spray. For most of the test runs, the model was set at a 5-deg angle of attack during the icing encounter. A diagram of the model mounted in the splitter walls is seen in Fig. 1.

The tunnel velocity at the location of the model was obtained by use of a calibration curve produced during earlier ground de-icing tests. This was done by relating a static pressure probe reading located at the model location, without the model present, to that of a static pressure probe located in the ceiling upstream of the splitter walls. The output of this probe was referenced to a heated total pressure probe, also located in the tunnel ceiling, to yield the corrected freestream velocity at the model location.

Aerodynamic loads on the models were measured during and after each test run using two three-component force balances. One balance was mounted in each splitter wall and attached to the end of the model. These balances allowed the measurement of the normal and axial forces and of the bending moment on the airfoil. From these measurements, the lift, drag, and pitching moment could be determined with an estimated accuracy of 3%.

During the de-icing/anti-icing test, a problem developed in the axial force component of the left-hand balance. This meant that any spanwise variation of the axial loading would lead to errors in the measurements. A simple examination of the relative magnitudes of the axial loads to either the lift or drag values indicated that an axial load imbalance could contribute to a 3% error in lift and as much as a 75% error in drag. It was decided to use the balance under these conditions and to take note of any test runs which had a nonuniform distribution of ice in the spanwise direction. It was felt that lift values would be acceptable and that if the ice accretion was uniform across the span, then the drag measurements would also be meaningful. This indeed was the case for most of the test runs. Three runs (run 21 is presented) had nonuniform ice accretions, and the drag data for these runs should be used with caution.

The test program consisted of 24 runs, 10 runs with the cruise configuration and 14 with the three high-lift configurations. Due to space considerations, seven test runs representing each of the configurations will be discussed in this article. The results for all tests will be available in a future document.

The test conditions were selected to simulate cruise and approach conditions for the Boeing 737-200ADV. This consisted of determining combinations of temperature, liquid water content, and drop size within the FAR-25 envelope and scaling these conditions to the size of the model, using scaling laws similar to those described by Ruff.[8] Velocities and accretion times were also adjusted in an attempt to achieve proper scaling of the total mass of ice accreted. The attempt to remain close to real flight conditions was done to produce realistic ice shapes but was not intended to achieve complete simulation of actual flight conditions. Since the main objective was to produce a data base for code validation, it was decided in several runs to deviate from the simulation conditions in order to produce ice accretions suitable for modeling. Typically the deviations consisted of running for longer periods of time in order to accumulate enough ice to yield a suitable shape for testing the computer codes. The actual test conditions are listed in the associated figures.

A typical test run consisted of the following steps. The force coefficients vs angle of attack were determined for the clean airfoil. The spray conditions were set and the tunnel was brought to the correct temperature and airspeed. As the spray was allowed to impinge on the airfoil, the force balance measurements were taken in order to determine changes during the encounter. These measurements were taken with the airfoil at a set angle of attack. Upon completion of the icing encounter, the force coefficients vs angle of attack were again taken to determine changes due to ice accretion and frost. After these measurements were completed, the tunnel was brought to idle, and frost was removed using plastic scrapers. The tunnel was then brought back to speed, and the force measurements were repeated with only the ice accretions.

After each icing test was conducted, a set of ice shape tracings were made at predetermined locations along the span of the airfoil. A steam knife was used to cut a 0.6-cm-wide slice into the ice and flush with the clean airfoil. Figure 1 shows the distance and section name for each of the five cuts.

Run number	Duration min.	Temperature °F	Velocity ft/s	LWC g/m^3	MVD um
4b	5	10	158	1.13	17

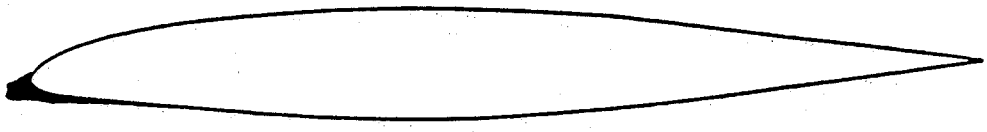

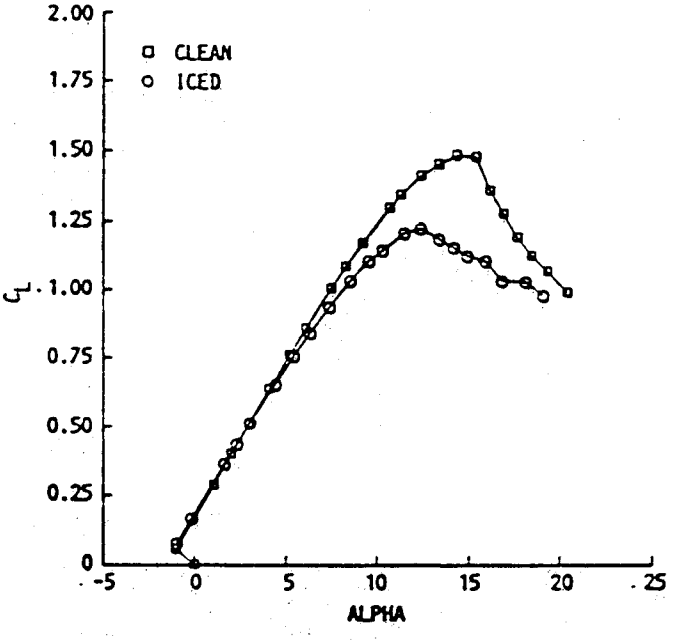

a) C_L vs AQA

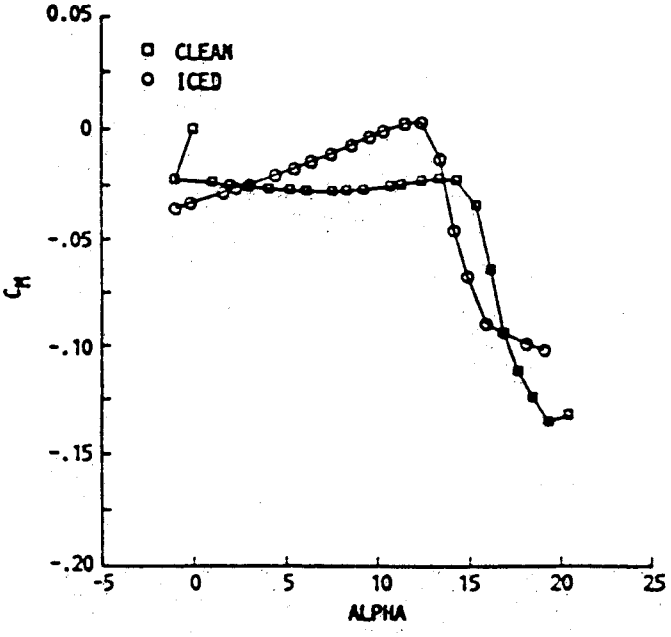

c) C_M vs AQA

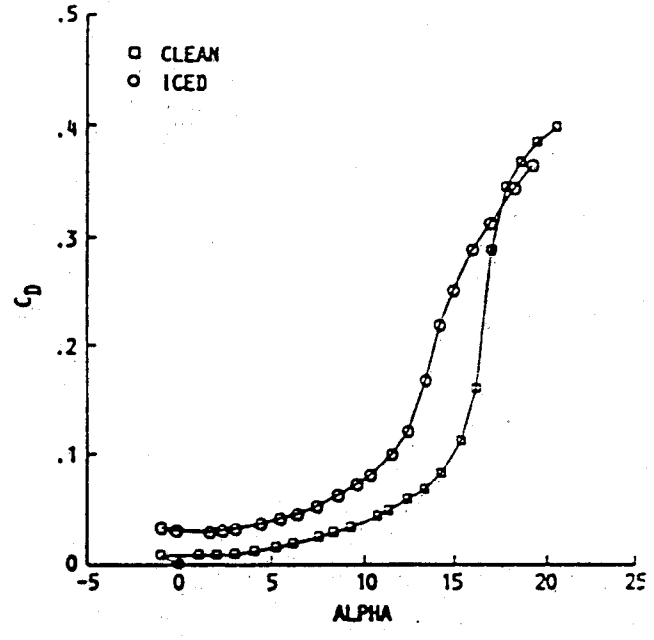

b) C_D vs AQA

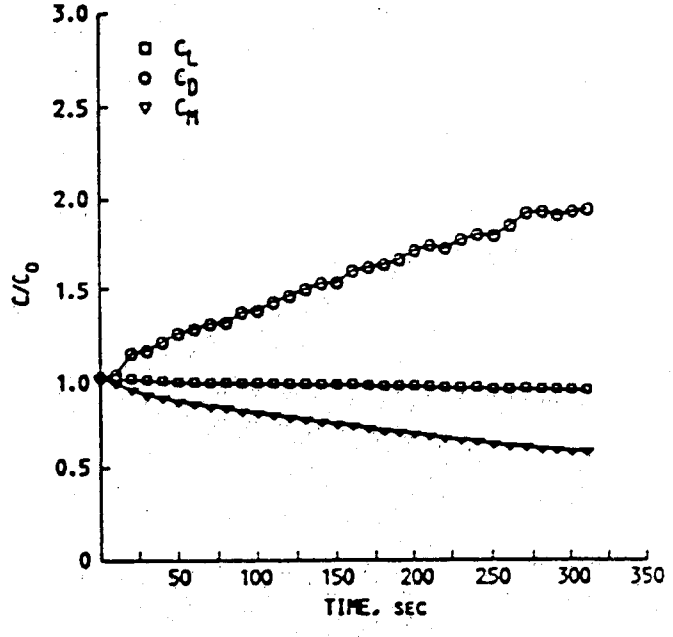

d) Ratio of force coefficients/force coefficient of clean airfoil vs time

Fig. 2 Ice shape tracings and force balance measurements for run number 4b.

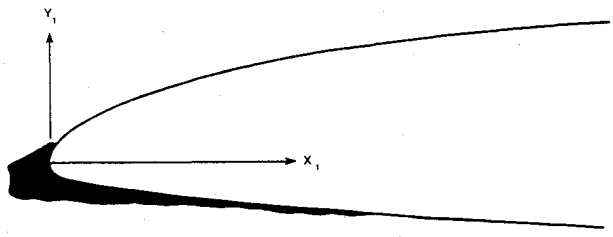

a) Leading edge

Fig. 3 Ice shape profiles for run number 4b.

After each cut was made, a cardboard template was inserted into the cut, and a tracing of the ice shape profile was made.

At the beginning of these tests, it was unclear if the splitter wall configuration (see Fig. 1) would significantly affect the flowfield and icing cloud near the wing especially if the splitter walls accreted a reasonable amount of ice during the run. Preliminary analysis, using LEWICE, indicated that the ice accretions that would form on the leading edge of the splitter walls would be less severe than the ice accretions that would form on the leading edge of the test model. Investigation of the ice shape tracings along the span of the airfoil indicated that the splitter walls did not have a significant effect on the ice shapes. Thus, it appeared that the splitter walls were not disturbing the flow downstream.

Results and Discussion of Test Program

The cruise wing configuration resulted in ice accretions near the leading edge as is typical for single-element airfoils. The high-lift configurations resulted in ice accretions at the flaps and slat leading edges. In some cases, the gaps between those surfaces and the main wing body were filled with ice. During many of the tests, frost also formed on the lower surface of the airfoil. The frost was especially evident for the 15-deg flap configuration. Frost was seen on the upper surface only in this latter configuration. In this case, there was a gap between the slat and the main wing body. Frost was distinguished from the actual ice accretions by its appearance. The ice accretions had a growth pattern that indicated development in the upstream direction. The frost on the other hand seemed to have no preferred direction for growth. Instead, the frost appeared as a thin layer with a uniformly rough surface. Olsen et al.[6] have suggested that the frost is due to a freestream turbulence level higher than that in flight. However, since only the lower surface of the airfoil had any frost, some other reason is suspected. The effect of the frost on the airfoil performance was evaluated by taking force measurements before and after removal of the frost.

The first series of tests were performed with the cruise wing configuration. Typical results are presented in Figs. 2 and 3, which show the ice shape tracing for run 4b, the force coefficients as a function of angle of attack, and the force coefficients as a function of time at 5-deg angle of attack. In general, the ice accretion produces a premature stall and increased drag. The drag values are larger over the entire range of angles whereas the lift is not generally affected until near $C_{L\max}$. This happens because the ice shape does not substantially alter the pressure distribution over the airfoil until flow separation occurs while the boundary layer is significantly altered at lower angles of attack. The moment coefficient changes from being nearly constant over the range of angle of attack to being a linearly increasing value with angle of attack until stall. Changes to this parameter reflect both the changes to the boundary layer at small angle-of-attack values and to the pressure distribution at large angles. All these results indicate significant changes in handling characteristics for the iced airfoil. Since the lift values do not change substantially until near $C_{L\max}$, this can be an extremely important result for incorporation into flight simulators.

The drag appeared to increase with time very rapidly during the initial change from clean surface to iced surface. Within the first minute, the rate of increase declined to a near-linear rise with time. The lift values did not change very much at all with time due to the low angle of attack at which the ice was accreted. The moment coefficient did not seem to follow any pattern in how it changed during the accretion time. Thus, it appears that as the ice accretes, it initially disturbs the boundary layer causing an increase in drag. This is most likely due to premature tripping from laminar to turbulent flow. Then, as the ice continues to grow, separation regions develop behind the ice shape, and changes to the boundary layer aft of the ice shape are reduced. Further changes to lift and pitching moment are determined not by the spray duration but by the type of ice accreted with the more significant changes occurring at the warmer temperatures. This latter effect is due to changes in the overall flow pattern as opposed to alterations in the boundary layer. These trends have been seen in other single-element airfoil studies and have been reproduced in analytical simulations.[9,10]

Frost developed on the lower surface of the airfoil. The extent of this frost varied from the first 30% of the airfoil to the entire lower surface. The major effect of frost is to increase the pitching moment over the entire range of angle of attack. The changes in lift and drag due to frost are not as dramatic, as will be seen in the next series of runs. This indicates that the results for lift and drag previously discussed should apply whether or not the frost is present.

Temperature influences the type of ice accreted on an airfoil surface. Temperatures close to freezing produce glaze ice accretions whereas lower temperatures produce rime ice accretions. The dramatic differences in airfoil performance resulting from these ice shapes is illustrated by comparing the results of runs 2b and 9, shown in Fig. 4. For these two runs the conditions were alike, except for the temperature. Run 2b, glaze ice accreted at $-2°C$, resulted in a change of $C_{L\max}$ from 1.5 to 0.95 and a decrease from 15 to 10 deg in the angle of attack at which $C_{L\max}$ occurs. For clean or iced conditions, the drag rises dramatically after stall. The ice shape causes this to occur earlier, thus aggravating the performance loss due to the decrease in lift. In contrast, run 9, rime ice accreted at $-27°C$, resulted in an enhancement to lift at angles of attack below stall. In this case, the rime ice accretion actually acted as a leading-edge slat. The $C_{L\max}$ value dropped from 1.5 to 1.35, a much smaller decrease than the glaze ice case. The drag rise is also less severe for this case.

The effects of an intermediate temperature condition are illustrated by the results of run 4b (see Fig. 2). In this case, the ice accretion consisted of a glaze ice core near the stagnation point with surrounding layers of rime ice. The lift curve does not exhibit the enhancement obtained in the rime ice run. The decrease in $C_{L\max}$, from 1.5 to 1.2, is intermediate to the changes due to the rime and glaze ice conditions. The drag rise for this run in the 10- to 15-deg angle-of-attack range. This is most likely due to early flow separation behind the glaze ice horn.

The 5-deg flap configuration is shown in Fig. 5. The distinguishing characteristic of these high-lift configurations is the sharp drop in lift at angles of attack near stall. The icing runs covered mixed to rime ice conditions, and these accretions altered the lift curve significantly. Results for run 14, shown in Figs. 5 and 6, indicate a change in the stall condition. The lift curve no longer has a sharp drop at 15 deg, indicative of a leading-edge stall, but rather has a gradual rollover suggesting an alternate stall mechanism. Apparently the ice shape causes early transition to turbulent flow resulting in trailing-edge separation. Confirmation of this would require pressure distributions and velocity profiles around the airfoil, which were not obtained for this experiment.

The other interesting feature of this set of runs is the effect

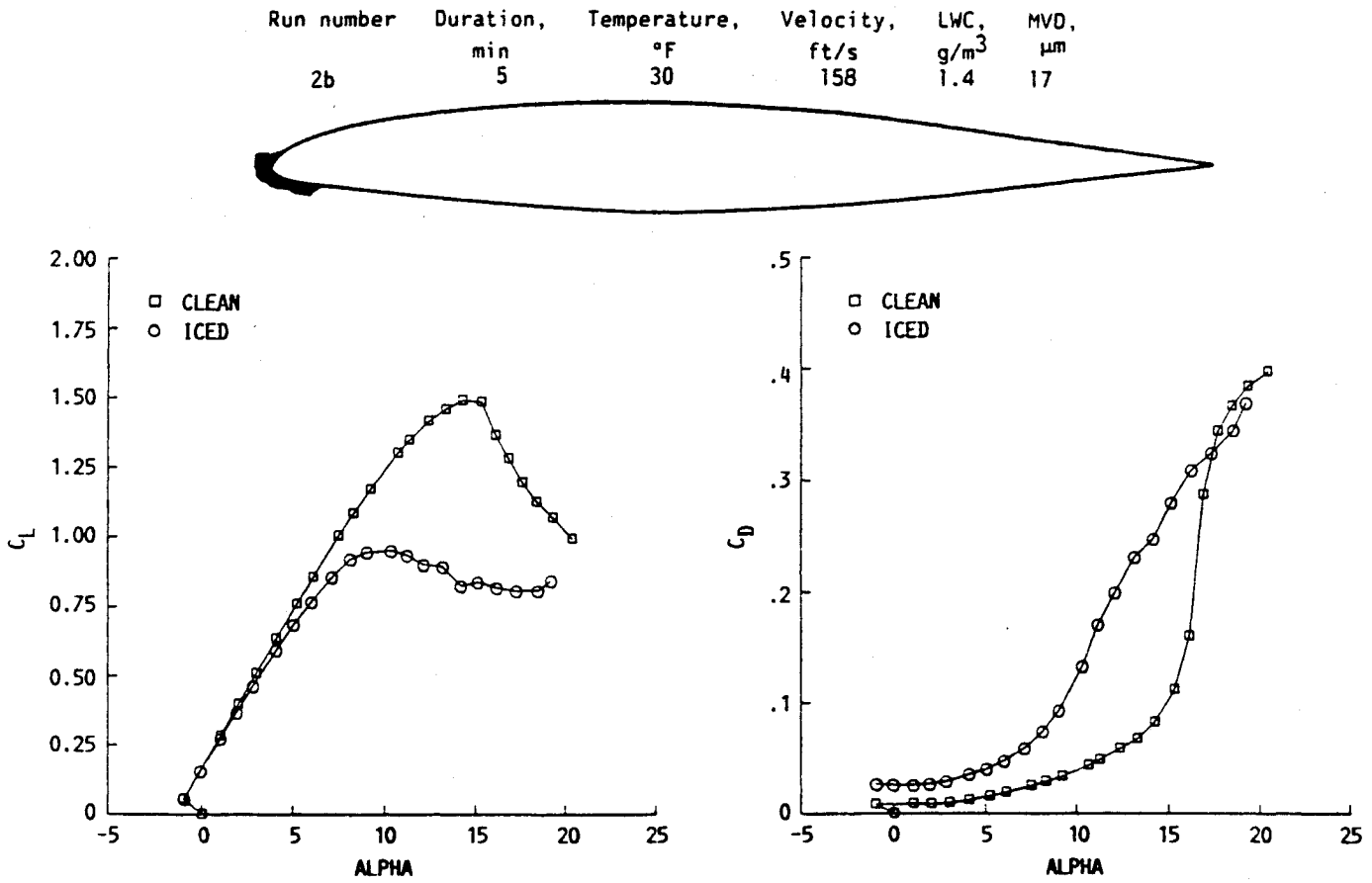

a) Ice shape tracings and force balance measurements for run number 2

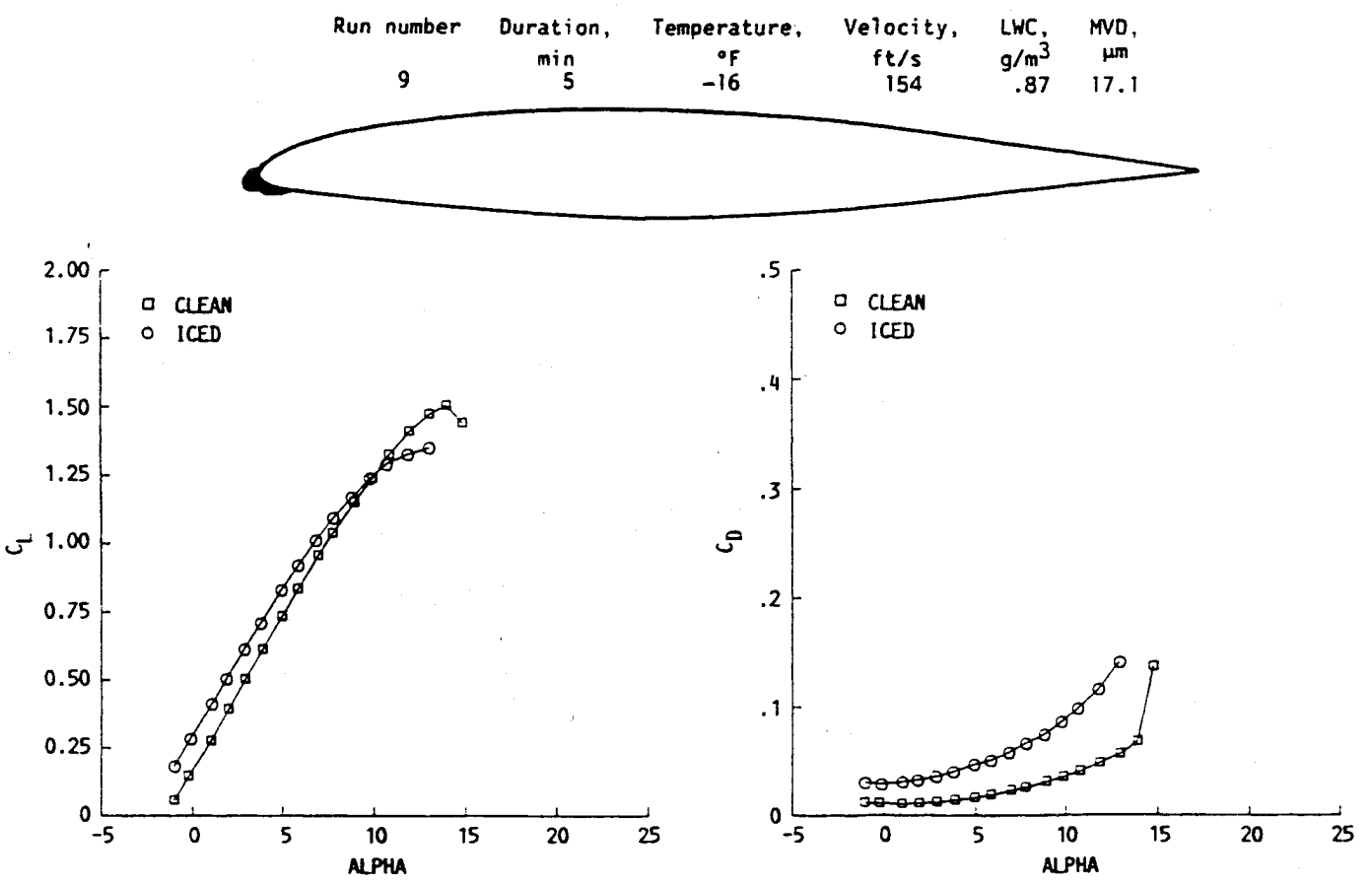

b) Ice shape tracings and force balance measurements for run number 9

Fig. 4 Comparison of ice shape tracings and force coefficients for run numbers 2b and 9.

Run number	Duration min.	Temperature °F	Velocity ft/s	LWC g/m^3	MVD um
14	8	-7	158	0.9	14

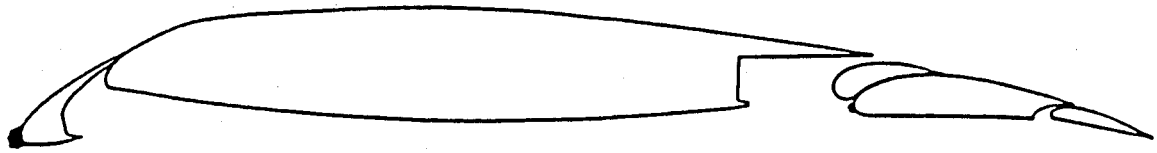

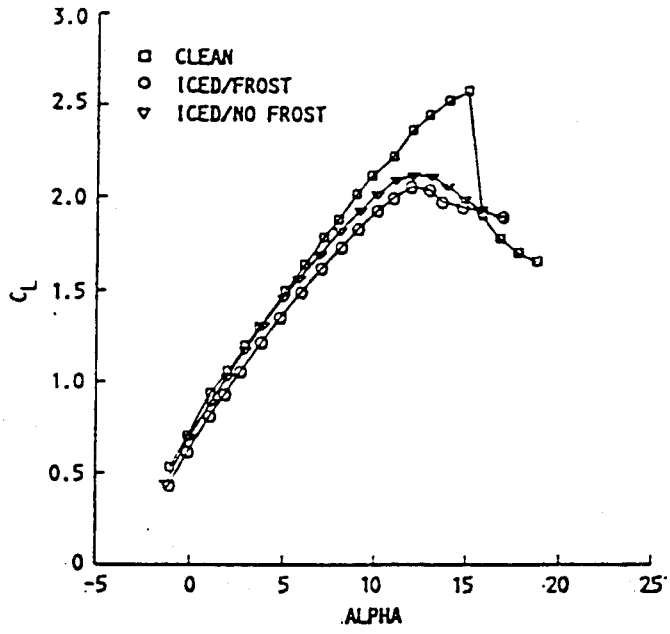

a) C_L vs AQA

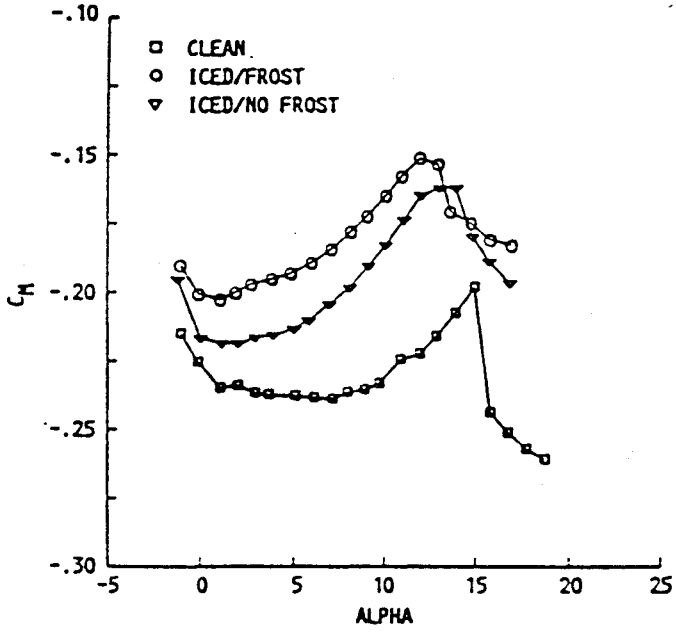

c) C_M vs AQA

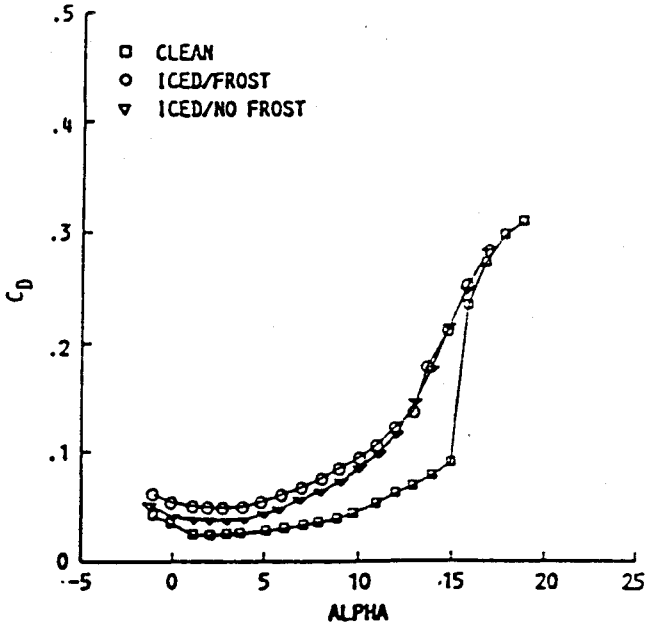

b) C_D vs AQA

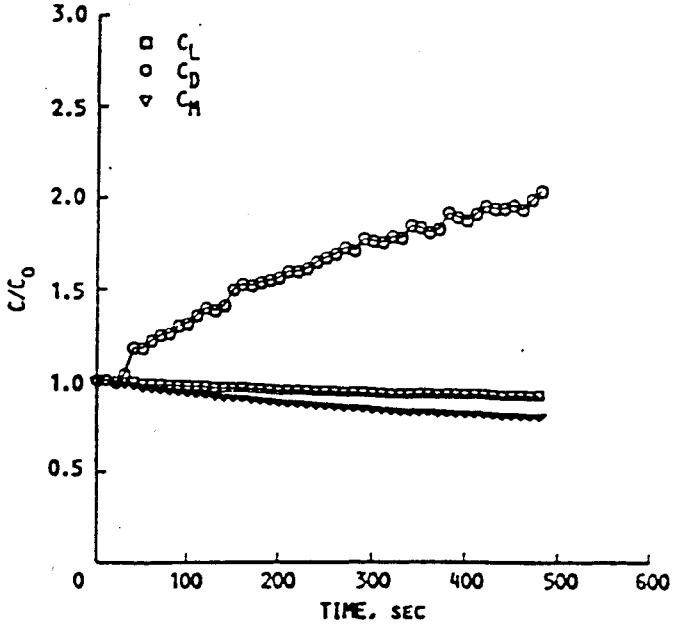

d) Ratio of force coefficients/force coefficient of clean airfoil vs time

Fig. 5 Ice shape tracings and force balance measurements for run number 14.

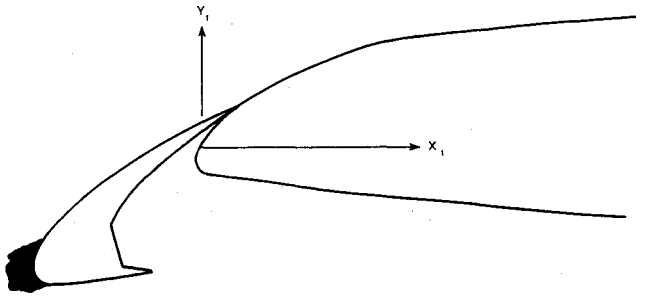

a) Leading edge slat

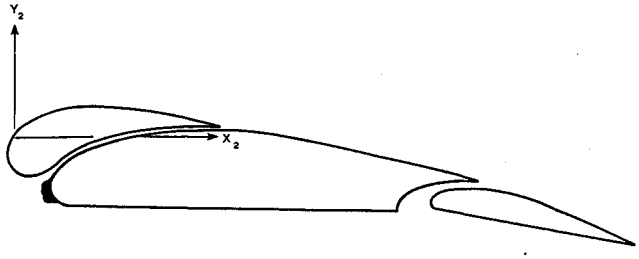

b) Trailing edge flaps

Fig. 6 Ice shape profiles for run number 14.

of the frost. As seen in Fig. 5, the lift and drag values were altered a little by the presence of the frost. On the other hand, the frost had a significant effect on the moment coefficient. The change in pitching moment is larger than would be suggested by the accompanying changes in lift and drag. Apparently the distribution of forces over the surface of the airfoil is changed by the frost. Since frost is considered to be a phenomenon found only in the tunnel and not in flight, tunnel tests must be evaluated with great care when extrapolating to airfoil performance in icing. This effect must also be considered when using tunnel data for code validation.

The 1-deg flap configuration, shown in Figs. 7 and 9, was evaluated during runs 15–19. The results for runs 19 and 17 are shown in Figs. 7 and 9, respectively. The ice shapes from these runs all tended to be on the upper surface of the leading-edge slat. This is quite different from the prior configurations where the ice accreted at the leading edge and on the lower surface. These runs produced lift curves with very flat tops such that stall would occur early but may not be as severe as other configurations. The drag and moment coefficient curves also appear to be affected similarly for all runs. All five of these runs were in the mixed ice regime and hence this could account for the similarities between runs.

Run 19 is particularly interesting due to the effect of frost on the lift and drag. In the range of a 10- to 15-deg angle of attack, the presence of frost makes a significant difference on both measurements. This run was the only one to have frost on the upper surface. The frost extended from the leading edge to the trailing edge of the main wing body. This appears to have thickened the boundary layer on the upper surface and possibly altered the pressure profile on the upper surface. This in turn resulted in the decreased lift and increased drag indicated in Fig. 7.

The effect of temperature on a high-lift configuration can be examined by comparing runs 17 and 19 (i.e., the clean and iced/no frost conditions only). These two runs correspond to glaze and mixed ice conditions, respectively. As in the cruise configuration, the lift decrease is greater for glaze conditions whereas the drag rise is approximately the same for both conditions. This indicates that the high-lift configuration is as susceptable to icing performance degradation as the cruise configuration. Unfortunately, there was no rime ice run for this configuration.

The last five runs were with the 15-deg flap configuration. The results for run 21 are shown in Figs. 10 and 11. There was no frost developed during this run; however, there was a thin layer of accreted ice on the lower surface of the main wing body. Additionally, ice deposits on the flaps were large enough to block the gaps between airfoil elements. The interesting aspect of these runs was the lift values at low angle of attack. Unlike the previous configurations, the lift values at angles of attack well below stall are lower than those of the clean airfoil. Obstruction of the flow over the flaps by the ice must have reduced the lift available from these elements. This could lead to a potentially more hazardous condition for this configuration. The stall condition is also altered by the ice accretion. The lift decreases more gradually than for the clean airfoil, and this decrease starts at a lower angle of attack. As suggested earlier, this is considered to be due to a change in stall mechanism from leading-edge stall to trailing-edge stall.

The variability of the ice shapes accreted during each run was examined by taking ice shape tracings at several spanwise locations as mentioned previously. The tracing locations are shown in Fig. 1. An example of the variability that can occur is indicated in Fig. 12a, which shows the tracings at all six locations for run 4b. Figure 12b gives an indication of the variability of the ice shape along the span for a given icing condition. Both the mass of ice and the extent of the ice along the surface can vary by as much as a factor of two. This degree of variability is within the scope of what would be considered a uniform ice shape as a result of visual inspection. If the ice accretion were visually nonuniform, then the variability could be an order of magnitude. Examination of photographs revealed that the ice accretion pattern consisted of many ribs of ice, each extending in a chordwise direction, along the span of the model. The limits of the ice accretion, shown in Fig. 12b, indicate tracings taken on and between these ribs. This run had one of the largest degrees of variability; other runs had tracings that literally overlapped. One other point to consider when evaluating these tracings is that the method of tracing a shape onto a template can itself cause some variability in determination of a given ice shape.

Ice Shape Tracing Compared to LEWICE Prediction

The NASA Lewis Research Center has directed the development of an analytical ice accretion prediction code to accurately predict the growth of ice on airfoils and other geometries. Initial development of the LEWICE code was provided through a grant to the University of Dayton Research Institute. This work was an extension of earlier work by Lozowski et al.[11] and Ackley and Templeton.[12] In 1984, the LEWICE code was brought in-house for further modifications and development. This effort resulted in a LEWICE User's Manual.[13] The LEWICE code consists of three main modules: 1) a potential flow panel method to calculate the flowfield about an arbitrary two-dimensional body; 2) a particle trajectory code that calculates the water droplet paths and their resulting impingement pattern on the body; and 3) an ice accretion module that solves the quasisteady energy balance equation. The energy balance equation first proposed by Messinger[12] accounts for the governing heat- and mass-transfer process occurring during the icing process. The LEWICE code is unique in that it has a time-stepping capability to grow the ice; other ice accretion codes grow the ice in one time step. With a time-stepping code, the flowfield and water droplet trajectories can be updated as ice is accreted on the leading edge, thus disturbing the flowfield. This should result in a more accurate representation of the flowfield as the ice accretion is formed. Inputs required by LEWICE include the cloud properties such as liquid water content (LWC) and droplet size (the actual cloud contains a distribution of droplet sizes which can be characterized by a median volumetric diameter, or MVD) and the icing conditions, which include the freestream velocity, static air temperature, static pressure, and the angle

Run number	Duration min.	Temperature °F	Velocity ft/s	LWC g/m^3	MVD um
19	10	19	157	0.9	14.4

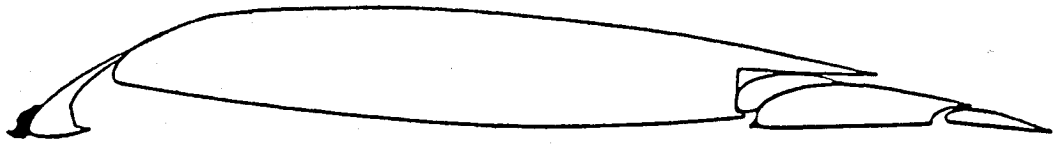

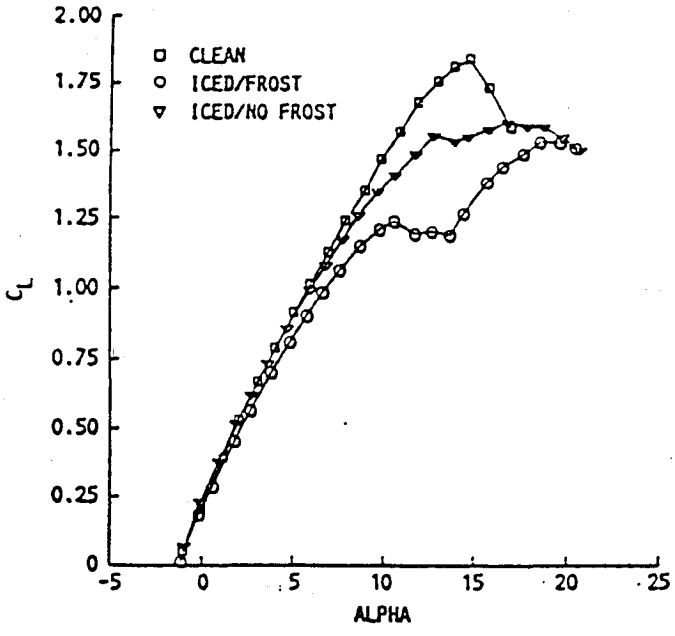

a) C_L vs AQA

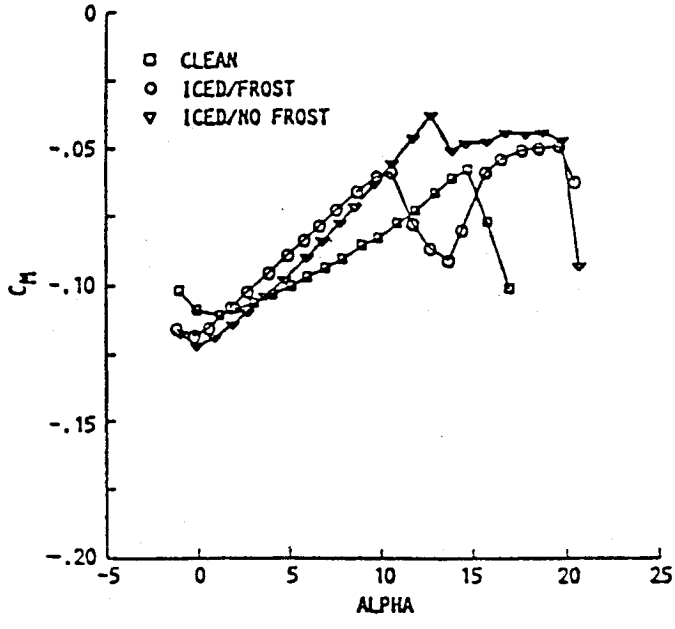

c) C_M vs AQA

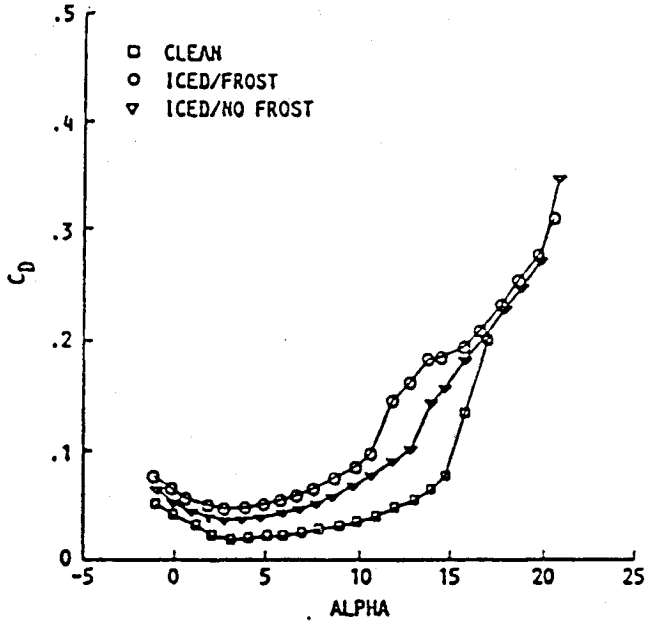

b) C_D vs AQA

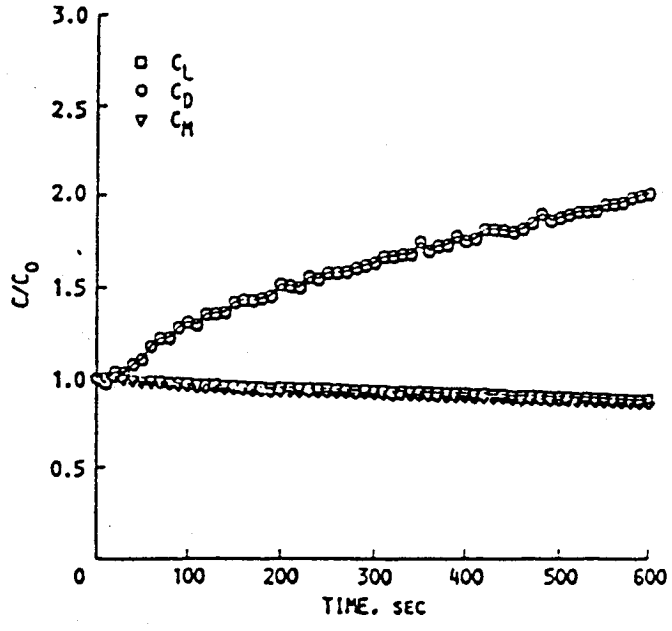

d) Ratio of force coefficients/force coefficient of clean airfoil vs time

Fig. 7 Ice shape tracings and force balance measurements for run number 19.

of attack. A detailed description of the code and the method of analysis can be found in the LEWICE User's Manual.[13]

To illustrate the utility of the LEWICE model, run 4b was selected as an example case in which the LEWICE-predicted ice shape will be compared to the experimental ice shape. Run 4b was selected for several reasons. First, the current LEWICE model has been tested with single-element airfoils only. Therefore, comparisons were limited to the cruise wing configuration. Second, run 4b had a relatively large ice accretion, and the performance characteristics of the airfoil indicated a significant degradation in lift between the clean and

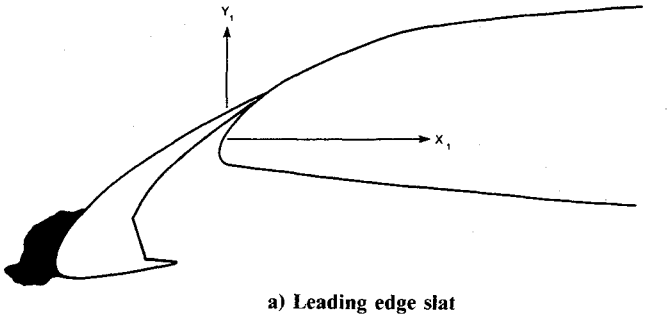

a) Leading edge slat

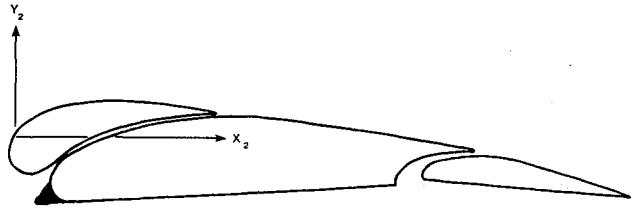

b) Trailing edge flaps

Fig. 8 Ice shape profiles for run number 19.

the iced airfoil geometries. Therefore, it was felt that this would be an interesting case not only for LEWICE but for performance calculations as well. Input values are shown in Fig. 13. LEWICE requires static temperature and pressure inputs that were calculated from the total temperature and pressure measurements. An airfoil chord of 45.72 cm was used along with an equivalent sandgrain roughness (k) of 0.08 cm. This value of k was determined from Ref. 13 (Appendix F) and is a function of the velocity, temperature, and liquid water content. For this comparison, two 2.5-min time steps were used to accrete the resultant ice shape. Figure 13a shows the predicted ice shape (solid line) and the experimental ice shape (dashed line) for run 4b. The experimental shape shown was taken from the center section of the airfoil, Sec. C_1. Generally speaking, LEWICE does a good job of predicting the ice shape. The calculated impingement limits and the mass of ice accreted agree quite well. However, the LEWICE-generated ice shape does not predict the "point" that exists near the leading edge of the experimental ice shape. The LEWICE prediction is also compared to the icing band discussed in the previous section (i.e., Fig. 13b), which indicates the variability of the ice shape along the span of the airfoil. The LEWICE prediction stays within the band everywhere except along the lower surface of the ice shape. This may be due to an excessive amount of water runback predicted by the code.

For the most part, Fig. 13 is typical of other LEWICE comparisons with both artificial and natural ice shape data. As other studies have indicated, LEWICE often provides a reasonable engineering approximation for most ice shapes. In general, LEWICE predictions agree more favorably with rime ice accretions than with glaze ice accretions, although results for glaze ice accretions are encouraging. For example, Berkowitz and Riley have indicated that LEWICE calculations were within 30% on the basis of volume of actual ice shapes obtained from tracings of ice accreted during a flight study.[13] There appears to be no set of icing conditions in which LEWICE consistently does a poor job. However, poorer

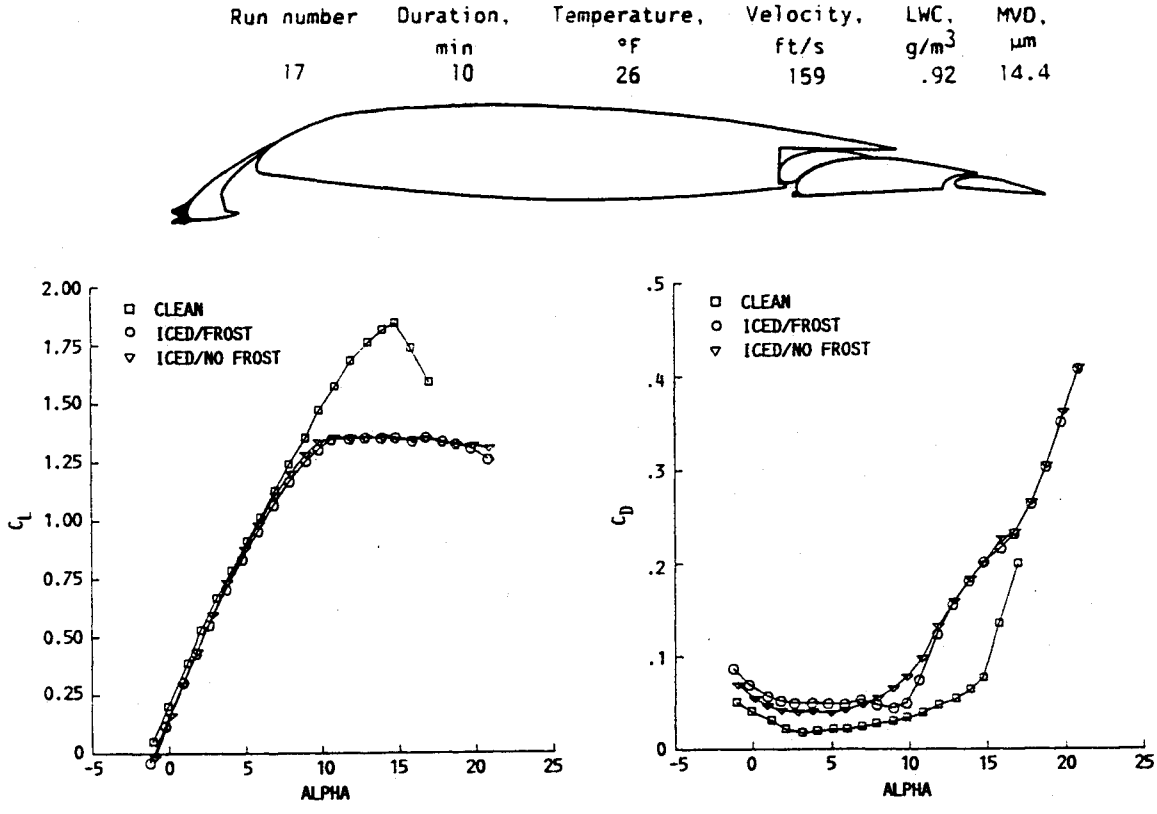

Fig. 9 Ice shape tracings and force balance measurements for run number 17.

Run number	Duration min.	Temperature °F	Velocity ft/s	LWC g/m^3	MVD um
21	8	28	158	0.92	14.4

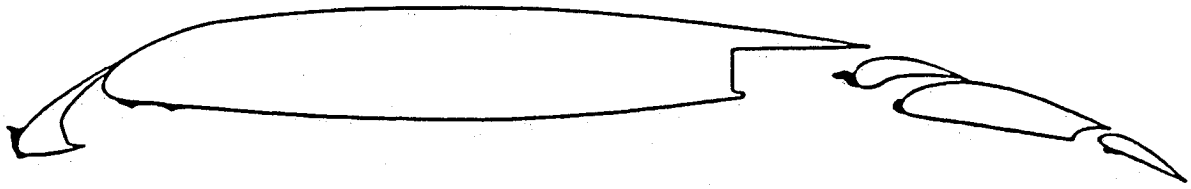

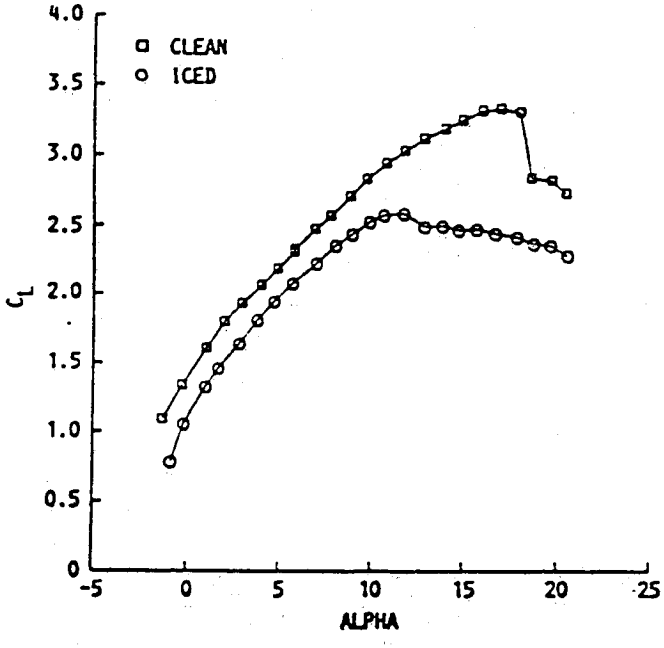

a) C_L vs AQA

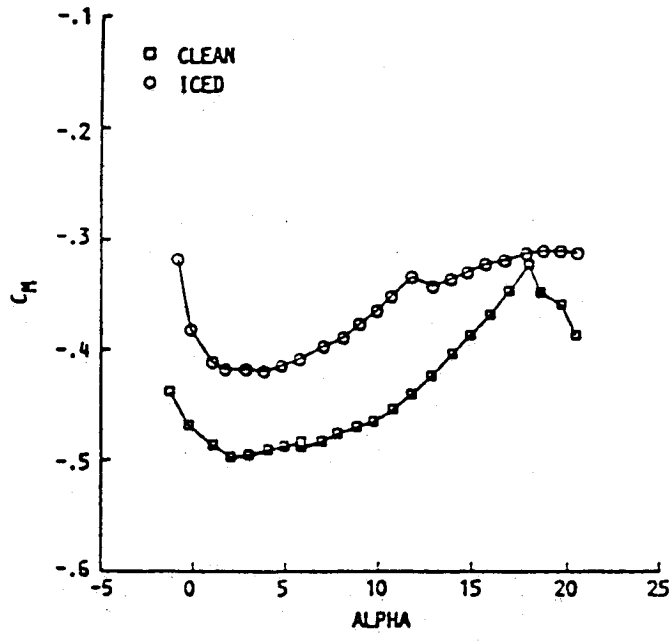

c) C_M vs AQA

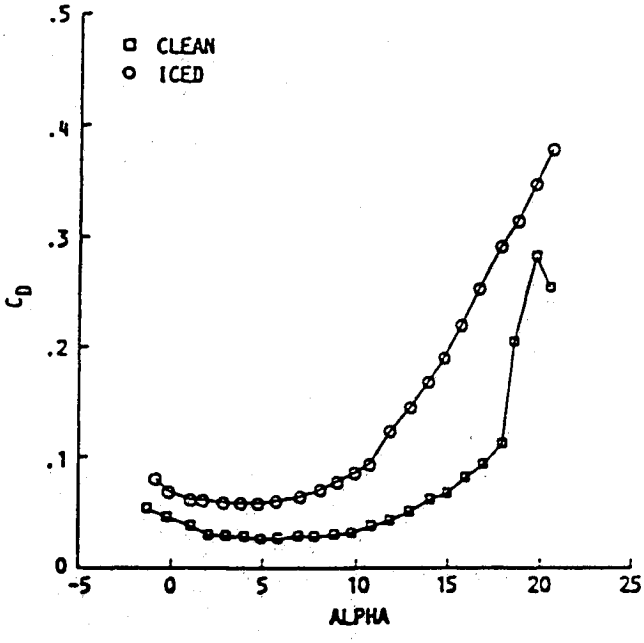

b) C_D vs AQA

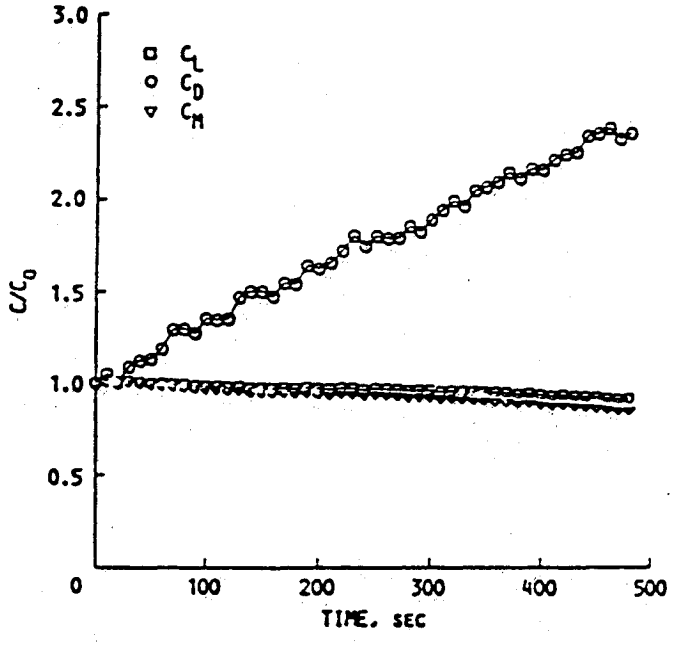

d) Ratio of force coefficients/force coefficient of clean airfoil vs time

Fig. 10 Ice shape tracings and force balance measurements for run number 21.

agreement will usually result for extreme cases such as large horn-shaped ice at high angles of attack. Recent high-speed films by Olsen and Walker[14] indicate that there may be some gross errors in the modeling of the physics of the ice accretion process, especially in the glaze ice regimes. This would explain the less than satisfactory results obtained from LEWICE for glaze ice comparisons. In addition, Hansman and Turnock[15] have proposed a multizone approach to the ice accretion process based on their experimental studies of the surface water behavior for glaze ice accretions. This and other work suggests that changes to the existing model should be made to try to improve the accuracy of the predictions. Investigation of these and other proposed modifications to the LEWICE model are currently being undertaken by the NASA Lewis Aircraft Icing Analysis Program.

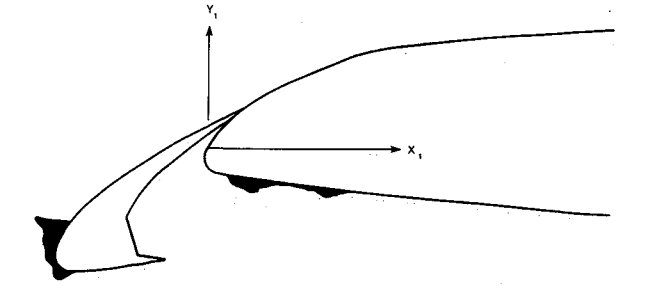

a) Leading edge slat

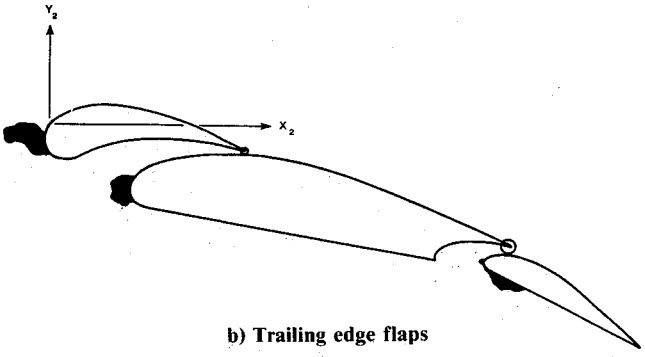

b) Trailing edge flaps

Fig. 11 Ice shape profiles for run number 21.

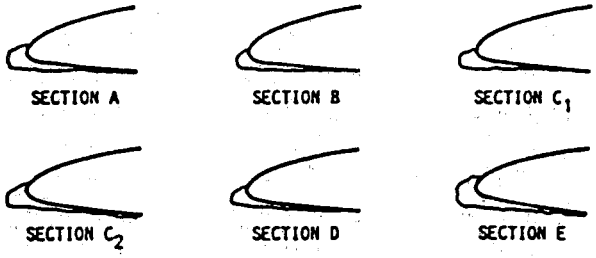

a) Ice shape tracings for section a-e

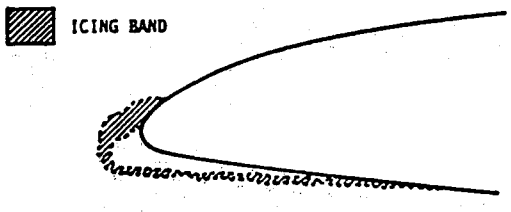

b) Composite of ice shape tracings showing icing band

Fig. 12 Spanwise variation in ice shapes for run 4b.

Performance Change Evaluation Using Navier-Stokes Code

Evaluation of the changes to airfoil performance resulting from ice deposition is a major goal in development of an icing analysis capability. Presently two methods are being considered. These are the interactive boundary-layer approach of Cebeci[9] and the use of a Navier-Stokes code.[10] For this work, the Navier-Stokes code, ARC2D,[18] was used to evaluate one of the test runs for changes in performance characteristics. The ARC2D solves the thin-layer form of the Navier-Stokes equations within a body-fitted coordinate system. An algebraic eddy viscosity model is used to provide representation of the turbulent flow behavior. A separate grid-generation code takes the iced airfoil geometry along with the dimensions of the surrounding physical space and produces the coordinate system used in the ARC2D code. The run 4b geometry was used for this calculation since this run was also chosen for use in the LEWICE evaluation.

Figure 14 provides the comparisons between ARC2D and experiment for both the clean airfoil and the iced airfoil. The calculations were extended to an angle of attack corresponding to $C_{L\max}$. For the clean airfoil, the agreement is excellent up to this point whereas at angles above $C_{L\max}$, the solution did not converge. Evaluation of this airfoil at these higher angles of attack will require further examination of such parameters as grid spacing or specification of the surface geometry. The results for the iced airfoil are not as good, with the code underpredicting the lift. The code results are for one cross section of the airfoil whereas the experimental results are for the entire wing section. Some method of incorporating the spanwise variation of the ice accretion geometry is required in order to capture the resulting changes in the aerodynamic forces. This could consist of using an "average" ice shape that represents the spanwise variation of calculating the forces for all six profiles and averaging the results. Additionally, further grid refinement may be required to adequately model this geometry. The use of tools such as an unstructured mesh are presently being examined. These results do indicate, however, that an actual ice shape geometry can be evaluated for changes in performance characteristics.

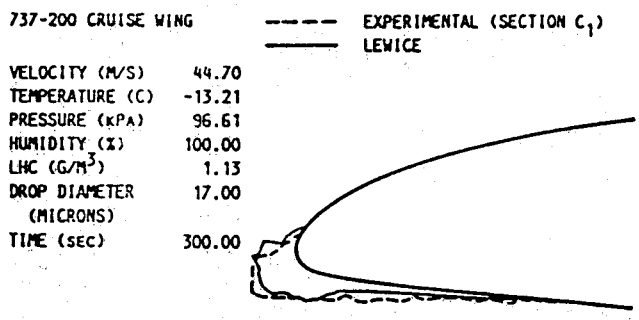

a) LEWICE comparison with section C_1

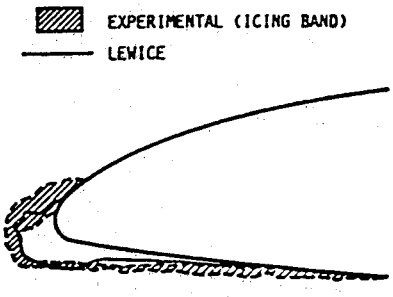

b) LEWICE comparison with icing band

Fig. 13 LEWICE comparison with experimental results for run 4b.

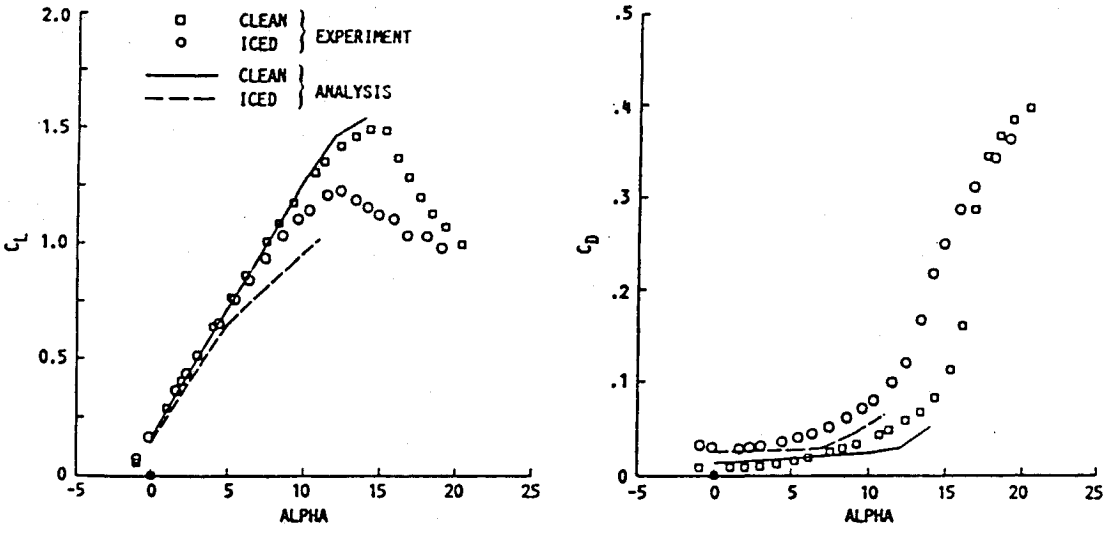

Fig. 14 Force coefficient comparisons between experimental results an analysis for cruise wing configuration, clean, iced; iced condition is run 4b.

Conclusions

This series of tests was designed to provide a verification data base for development of multielement airfoil ice accretion codes and aerodynamic performance codes. The test results provide a wide variety of conditions and should serve as a set of useful test cases. The single-element airfoil cases help to ensure confidence in the capabilities of the codes prior to modification for multielement geometries.

The test results indicate that the changes in performance characteristics are most affected by the temperature and duration of the ice accretion. The warmer temperatures, leading to glaze ice conditions, tend to produce the largest loss of lift. The duration of the accretion does not influence the changes to the lift, as shown in the lift history plots, once the accretion has developed beyond some minimal size. The drag increase is not so dependent on temperature although it does increase significantly with time. The drag rise was seen to rise rapidly during the initial change from a clean condition to an iced condition with a linear increase thereafter. The moment coefficient normally increased as a result of the accretion. This tended to produce a less stable condition for the airfoil as the tendency toward stall was enhanced.

Test results indicate that performance changes due to icing can be dependent on the airfoil configuration. For the cruise configuration and the 1-deg flap configuration, the performance changes due to glaze or mixed ice accretions were similar. The cruise configuration actually had increased lift as a result of rime ice accretion with the ice acting as a leading-edge slat. It is doubtful that this would occur for the other configurations. The 15-deg flap configuration accumulated ice on the flaps, which resulted in lift loss for all angle-of-attack conditions. This indicates that high-lift configurations may be more sensitive to icing problems than cruise configurations. This suggests that an airplane is most sensitive to icing performance losses just at the time it is most likely to experience icing conditions.

Another significant result was documentation of the effect of frost. Frost was identified as ice that developed with no preferred growth direction as opposed to accreted ice that tended to grow upstream. Typically, the frost grew on the first 30–40% of the lower surface of the airfoil. The frost did not alter the lift or drag in many cases but did change the pitching moment. This indicates that the pressure profile was altered somewhat but more in distribution than in magnitude. It is important to insure that frost is removed prior to measurement of iced airfoil performance values in order to more accurately recreate natural icing conditions.

Variability of the ice accretion as a function of spanwise location was documented by taking ice shape profile tracings at several locations during each test run. Results indicated that the ice shape profiles could be quite different even when visual inspection indicated uniform ice growth. This suggests that ice accretion codes, such as LEWICE, be compared to more than one specific profile for a given set of icing conditions. As such, the LEWICE comparison to run 4b indicated that the code prediction fell within the icing band constructed from all the tracing of that test. The test also provided data useful for evaluation of performance-change calculations with a multielement airfoil code.

Acknowledgment

Design and construction of the model and splitter walls was performed by Boeing Commercial Aircraft Co. in conjunction with their own fluid de-icing test conducted just prior to the test described herein.

References

[1]Gray, V. H., and von Glahn, U. H., "Effects of Ice and Frost Formations on Drag of NACA 65-212 Airfoil for Various Modes of Thermal Ice Protection," NACA TN-2962, June 1953.

[2]Gray, V. H., and von Glahn, U. H., "Aerodynamic Effects Caused by Icing of an Unswept NACA 65A004 Airfoil," NACA TN-4155, Feb. 1958.

[3]Bragg, M. B., Zaguli, R. J., and Gregorek, G. M., "Wind Tunnel Evaluation of Airfoil Performance Using Simulated Ice Shapes," NASA CR-167960, Nov. 1982.

[4]Korkan, K. D., Cross, E. J., Jr., and Cornell, C. C., "Experimental Study of Performance Degradation of a Model Helicopter Main Rotor with Simulated Ice Shape," AIAA Paper 84-0184, Jan. 1984.

[5]Bragg, M. B., "An Experimental Study of a NACA 0012 Airfoil with a Simulated Glaze Ice Accretion," Ohio State Univ., Columbus, OH, Rept. AARL 8602 (to be published as a NASA CR).

[6]Olsen, W., Shaw, R., and Newton, J., "Ice Shapes and the Resulting Drag Increase for a NACA 0012 Airfoil," NASA TM-83556, Jan. 1983.

[7]Ingelman-Sundberg, M., Trunov, O. K., and Ivaniko, A., "Methods for Prediction of the Influence of Ice on Aircraft Flying Characteristics," Joint Swedish-Soviet Working Group on Aircraft Swedish-Soviet Working Group on Aircraft Safety, JR-1, 1977.

[8]Ruff, G., "Analysis and Verification of the Icing Scaling Equations," AEDC-TR-85-30, Vol. 1 (revised), March 1986.

[9]Cebeci, T., "Prediction of Flow Over Airfoils with Leading Edge Ice," AIAA Paper 88-0112, Jan. 1988.

[10]Potapczuk, M. G., "Navier-Stokes Computations for NACA

0012 Airfoil with Leading Edge Ice," AIAA Paper 87-0101, Jan. 1987.

[11]Lozowski, E. P., Stallabrass, J. R., and Hearty, P. F., "The Icing of an Unheated Non-Rotating Cylinder. Pt. 1: A Simulation Model," *Journal of Climatology and Applied Meteorology*, Vol. 22, No. 12, 1983, pp. 2053–2062.

[12]Ackley, S. F., and Templeton, M. K., "Computer Modeling of Atmospheric Ice Accretion," Cold Regions Research and Engineering Laboratory Report 79-4, March 1979.

[13]Ruff, G. A., and Berkowitz, B. M., "User's Manual for the NASA Lewis Ice Accretion Prediction Code (LEWICE)," NASA CR-185129, May 1990.

[14]Messinger, B. L., "Equilibrium Temperature of an Unheated Icing Surface as a Function of Airspeed," *Journal of Aeronautical Science*, Vol. 20, No. 1, 1953, pp. 29–42.

[15]Berkowitz, B. M., and Riley, J. T., "Analytical Ice Shape Predictions for Flight in Natural Icing Conditions," NASA CR-182234, Dec. 1988.

[16]Olsen, W. A., Jr., and Walker, E. D., "Experimental Evidence for Modifying the Current Physical Model for Ice Accretion on Airfoil Surfaces," NASA TM-87184, May 1986.

[17]Hansman, R. J., Jr., and Turnock, S. R., "Investigation of Surface Water Behavior During Glaze Ice Accretion," AIAA Paper 88-0015, Jan. 1988.

[18]Pulliam, T. H., "Euler and Thin-Layer Navier-Stokes Codes: ARC2D, ARC3D," *Notes for Computational Fluid Dynamics User's Workshop*, The University of Tennessee Space Institute, Tullahoma, TN, March 1984.